

UCSF

UC San Francisco Previously Published Works

Title

Sp9 Regulates Medial Ganglionic Eminence-Derived Cortical Interneuron Development.

Permalink

<https://escholarship.org/uc/item/6056b3k7>

Journal

Cerebral Cortex, 29(6)

ISSN

1047-3211

Authors

Liu, Zhidong
Zhang, Zhuangzhi
Lindtner, Susan
et al.

Publication Date

2019-06-01


DOI

10.1093/cercor/bhy133


Peer reviewed

ORIGINAL ARTICLE

Sp9 Regulates Medial Ganglionic Eminence-Derived Cortical Interneuron Development

Zhidong Liu¹, Zhuangzhi Zhang¹, Susan Lindtner², Zhenmeiyu Li¹, Zhejun Xu¹, Song Wei¹, Qifei Liang¹, Yan Wen¹, Guangxu Tao¹, Yan You¹, Bin Chen³, Yanling Wang⁴, John L. Rubenstein² and Zhengang Yang ¹

¹State Key Laboratory of Medical Neurobiology, Department of Neurology, Institutes of Brain Science, Zhongshan Hospital, Fudan University, Shanghai 200032, China, ²Nina Ireland Laboratory of Developmental Neurobiology, Department of Psychiatry, UCSF Weill Institute for Neurosciences, University of California, San Francisco, San Francisco, CA 94158, USA, ³Department of Molecular, Cell and Developmental Biology, University of California, Santa Cruz, Santa Cruz, CA 95064, USA and ⁴Department of Neurological Sciences, Rush University Medical Center, Rush University, Chicago, IL 60612, USA

Address correspondence to Zhengang Yang, State Key Laboratory of Medical Neurobiology, Department of Neurology, Institutes of Brain Science, Zhongshan Hospital, Fudan University, 138 Yi Xue Yuan Road, Shanghai 200032, China. Email: yangz@fudan.edu.cn  orcid.org/0000-0003-2447-6540

Zhidong Liu and Zhuangzhi Zhang contributed equally to this work

Abstract

Immature neurons generated by the subpallial MGE tangentially migrate to the cortex where they become parvalbumin-expressing (PV⁺) and somatostatin (SST⁺) interneurons. Here, we show that the Sp9 transcription factor controls the development of MGE-derived cortical interneurons. SP9 is expressed in the MGE subventricular zone and in MGE-derived migrating interneurons. Sp9 null and conditional mutant mice have approximately 50% reduction of MGE-derived cortical interneurons, an ectopic aggregation of MGE-derived neurons in the embryonic ventral telencephalon, and an increased ratio of SST⁺/PV⁺ cortical interneurons. RNA-Seq and SP9 ChIP-Seq reveal that SP9 regulates MGE-derived cortical interneuron development through controlling the expression of key transcription factors *Arx*, *Lhx6*, *Lhx8*, *Nkx2-1*, and *Zeb2* involved in interneuron development, as well as genes implicated in regulating interneuron migration *Acr3*, *Epha3*, and *St18*. Thus, Sp9 has a central transcriptional role in MGE-derived cortical interneuron development.

Key words: interneurons, *Lhx6*, *Lhx8*, medial ganglionic eminence, *Nkx2-1*, parvalbumin, somatostatin, Sp9, tangential migration

Introduction

The subpallium consists of the lateral, medial, and caudal ganglionic eminences (LGE, MGE, and CGE, respectively) and the preoptic area (POA). The MGE and CGE generate the vast majority of mammalian cortical interneurons. The MGE generates parvalbumin (PV⁺) and somatostatin (SST⁺) cortical interneurons, which constitute about 60% of the total (Wonders and Anderson 2006; Gelman and Marin 2010; Rubin et al. 2010;

Brown et al. 2011; Rudy et al. 2011; Taniguchi et al. 2013). The MGE also generates striatal GABAergic and cholinergic interneurons and pallidal projection neurons (e.g., the globus pallidus) (Marin et al. 2000; Flandin et al. 2010; Nobrega-Pereira et al. 2010; Wang et al. 2014).

A cascade of transcription factors regulates MGE identity and differentiation. In ventricular zone (VZ) cells (radial glia), *Nkx2-1* and *Otx2* specify MGE regional identity (Sussel et al.

1999; Butt et al. 2005; Flandin et al. 2010; Hoch et al. 2015; Nord et al. 2015; Silberberg et al. 2016). *Otx2* represses ventral identity (POA), whereas *Nkx2-1* represses dorsal and caudal identities (LGE and CGE). In addition, *Otx2* promotes radial glia maturation into neurons and oligodendrocytes (Hoch et al. 2015) and *Nkx2-1* promotes the expression of subventricular zone (SVZ) (secondary progenitors) genes essential for neuronal differentiation (*Lhx6* and *Lhx8*) and patterning/survival (*Shh*) (Sussel et al. 1999; Du et al. 2008; Silberberg et al. 2016). *Nkx2-1* expression needs to be extinguished for interneurons to migrate to the cortex (Nobrega-Pereira et al. 2008); this is controlled in part via *Dlx1&2* induction of *Zeb2* (*Zfhx1b*, *Sip1*) (McKinsey et al. 2013; van den Berghe et al. 2013). *Lhx6* is required for the differentiation of GABAergic PV⁺ and SST⁺ cortical interneurons (Alifragis et al. 2004; Liodis et al. 2007; Zhao et al. 2008; Neves et al. 2013). *Lhx6* drives the expression of *Arx* and *Ackr3* (*Cxcr7*) to regulate cortical interneuron differentiation and migration, respectively (Vogt et al. 2014). *Lhx8* is required for the differentiation of striatal cholinergic neurons (Zhao et al. 2003; Fragkouli et al. 2005, 2009). *Lhx6* and *Lhx8* are partially redundant, and lacking both causes severe pallidal defects, including loss of *Shh* expression in pallidal neurons which reduces late-born cortical interneurons, and upregulation of *Nkx2-1* expression in a subset of MGE-derived interneurons which induces an ectopic aggregation of them in the ventral telencephalon (Flandin et al. 2011).

Much of the progress in understanding how the MGE generates interneurons and projection neurons has come from the analysis of genes downstream of *Dlx1&2* (Anderson et al. 1997; Long, Cobos, et al. 2009; Long, Swan, et al. 2009). The zinc finger transcription factor *Sp9* is particularly interesting because its expression is similar to *Dlx1&2* in the SVZ of the GE, and yet its function and targets in the MGE are unknown. In the ventral LGE, *Sp9* expression persists in striatopallidal medium-spiny neurons; its function is required for the generation, differentiation and postnatal survival of striatopallidal neurons (Zhang et al. 2016). In the dorsal LGE and postnatal SVZ, *Sp9* and *Sp8* coordinately regulate the development of olfactory bulb interneurons (Li et al. 2017). Here, we provide evidence that *Sp9* regulates MGE-derived interneuron tangential migration in part through promoting *Lhx6* expression. Deletion of *Sp9* results in ectopic aggregation of MGE-derived interneurons in the embryonic ventral telencephalon, and approximately 50% reduction of MGE-derived cortical interneurons.

Materials and Methods

Mice

Mice were handled in accordance with the institutional guidelines. *Nkx2-1-Cre* (Xu et al. 2008), *Lhx6-Cre* (Fogarty et al. 2007), *Rosa-YFP* (Srinivas et al. 2001), *Sp9^{LacZ/+}* (Zhang et al. 2016), and *Sp9^{Flox/+}* (Zhang et al. 2016) mice were previously described. The day of vaginal plug detection was defined as embryonic day 0.5 (E0.5).

Immunohistochemistry

Immunohistochemistry was performed on 12 μm (embryonic brains) or 30 μm (postnatal brains) coronal sections according to previous studies (Zhang et al. 2016; Li et al. 2017). Briefly, sections were rinsed in TBS (0.01 M Tris-HCL + 0.9% NaCl, pH = 7.4), blocked with 5% donkey serum/TBS, and then incubated overnight at 4 °C with primary antibodies as followed: rabbit anti-*Sp9* (1:500) (Zhang et al. 2016), rabbit anti-calretinin (CR) (1:3000,

AB5054, Millipore), chicken anti-GFP (1:2000, GFP-1020, Aves labs), rabbit anti-PV (1:2000, PV25, Swant), rabbit anti-*Nkx2-1* (1:500, sc-13 040, Santa Cruz), rabbit anti-Caspase-3 (1:300, 9661, Cell Signaling), goat anti-ChAT (1:400, AB144P, Millipore), mouse anti-*Lhx6* (1:500, sc-271 433, Santa Cruz), rabbit anti-NPY (1:500, 22 940, Incstar), and goat anti-SST (1:500, sc-7819, Santa Cruz). Sections were then incubated with secondary antibodies (1:400, Jackson ImmunoResearch) for 2–3 h at room temperature.

In situ Hybridization

RNA in situ hybridization experiments were performed using digoxigenin riboprobes on 20-μm cryostat coronal sections as previously described (Long, Cobos et al. 2009; Long, Swan et al. 2009; McKinsey et al. 2013; Zhang et al. 2016; Li et al. 2017). Riboprobe templates were amplified by PCR with the following primers:

1. *Lhx6* Fwd: CAGAGAGGGCGCGCATGGTCACT
Lhx6 Rev: AATTGGGGGGGGTCTTTGGCAC
2. *Lhx8* Fwd: GCCTTAGTGTGGCTGAGAGA
Lhx8 Rev: AGGATGGTAGGCTTTGAAACT
3. *Shh* Fwd: ACAGCTCACAAGTCCCTCAGGTT
Shh Rev: CGTCTCGATCACGTAGAAGACC
4. *Ackr3* Fwd: ATGGATGTGCACTTGTTTGACTATG
Ackr3 Rev: GTTCTGTCCAGGGCAGAGTACTC
5. *Maf* Fwd: GCGCACCTGGAAGACTACTACTGGA
Maf Rev: CTCCTTGTAGGCGTCCCTTTTCG
6. *Arx* Fwd: ATGAGCAATCAGTACCAGGAAGAGG
Arx Rev: TTAGCACACCTCCTTCCCGT
7. *Sp9* Fwd: ACCTGAATCGTGATTCCCAGCAG
Sp9 Rev: TGCTATGGCTTTTGAACCCAC
8. *Sp8* Fwd: TGGGTTGTCTGGTGAACAGTG
Sp8 Rev: CGAAGCAGAGGAAAACACTATCT
9. *NPY* Fwd: GTGGATCTCTCTCAGAGGGCA
NPY Rev: ACAACAACAACAAGGAAATGG
10. *Rnd2* Fwd: AGAGTGGCCGCTGCAAGATC
Rnd2 Rev: TCACATGAGGTTACAGCTCTTGGC
11. *Epha3* Fwd: GTCACCTATGTTCTGGTGGGGAG
Epha3 Rev: CCTCATGCCGTTAAGCCAATCAC
12. *Zeb2* Fwd: GCAAATGCTATGACTTAGCTCCCG
Zeb2 Rev: AAGTAGCGGTGAGTCACATCCAGG
13. *Sox6* Fwd: AACTCGGCAGGGGCAGTCT
Sox6 Rev: CGCTGCTATAGCTGATTGGGATC
14. *Id2* Fwd: GGTCTTCCTCCTACGAGCAGCA
Id2 Rev: CTGGTTGTCTGAAATAAAGCAAGCA
15. *Dlx2* Fwd: TTTCTGTCCCGGTCAGGAT
Dlx2 Rev: AAGTCTCAGACGCTGTCCACTCGA
16. *Ccnd2* Fwd: CCCAAGCTTGGGCTAGCAGATGACGAACACG
Ccnd2 Rev: GCTCTAGATCCCATTAGCCAAAGGAAGGA

RNA-Sequencing (RNA-Seq)

The MGEs from E12.5 *Sp9^{LacZ/LacZ}* null mutant and wild-type brains ($n = 3$ per group) were dissected, and RNA was isolated with the Direct-zol RNA Miniprep kit (Zymo, catalog #R2050) following the manufacturer's instructions (Li et al. 2017). The values of gene expression level were reported in fragments per kilobase of exon model per million mapped reads (Trapnell et al. 2012). For a gene to be called as differentially expressed, it required a P-value <0.05. RNA data from this experiment has been deposited in the GEO database (GSE99049).

ChIP-Seq

SP9 ChIP-seq was performed using dissected E13.5 lateral and medial ganglionic eminences (MGE) (including VZ, SVZ, and marginal zone, MZ) of wild-type CD1 mice ($n = 2$ replicas, 2 liters for each independent ChIP experiment) (Sandberg et al. 2016; Pla et al. 2017). Briefly, the E13.5 ganglionic eminences were fixed in 10 ml 1% formaldehyde for 10 min. Sonication was performed using Bioruptor[®] Pico (15–20 cycles) to obtain optimal fragment size in the range of 200–500 bp. The sheared chromatin (SDS concentration diluted to 0.1%) was incubated with 8 μ g anti-SP9 rabbit polyclonal antibody at 4 °C overnight. ChIP-seq sequencing libraries were prepared from both the input DNA and the precipitated DNA using the NEBNext DNA Library Prep Kit and Illumina standard adaptors and were sequenced on the Illumina HiSeq 4000 with 150 bp pair-end reads. Reads from the ChIP and input libraries were mapped to the mouse genome (mm9) using Bowtie with default parameters. Peaks were called considering input as the control sample with filtering to remove peaks in repeat regions. ChIP-seq peaks were visualized using the UCSC genome browser.

Luciferase Assays

The DNA fragments of *Lhx6* promoter, *Lhx6* and *Lhx8* putative enhancers (region 1–3) were amplified by PCR and subsequently cloned into pGL4.10 and pGL4.23 firefly luciferase vector (Promega) upstream of *Luc2* gene, respectively (McKinsey et al. 2013).

The primers used for amplifying the *Lhx6* promoter were:

Fwd: 5'-CCTGTTATATAAACCGGCGCTGAAC-3'
Rev: 5'-ACCGATTTAGCAAAGACATAGCGGA-3'

The primers used for amplifying the *Lhx6* putative enhancers (Region 1 and Region 2) and the *Lhx8* putative enhancer (Region 3) were the following:

Region 1 Fwd: 5'-TCTAGACCTGGGAGAGACACACACG-3'
Rev: 5'-AGCCATTTTCACTCTCTCCGAAGAA-3'
Region 2 Fwd: 5'-GGAAACCTCAAGCTGCTCTTCGTAG-3'
Rev: 5'-GAGACCCACCAGCTAGTTGCTAAAA-3'
Region 3 Fwd: 5'-AGCGGGCGACTCGAGGACT-3'
Rev: 5'-ACTGAGCACTAAGTGGCAATTCACA-3'

The coding sequence (CDS) of *Sp9* was amplified by PCR from mouse genomic DNA and cloned into pCS2 (+) expression vector, using the following primers:

Sp9 CDS Fwd: 5'-GACCTGAATCGTGATTCAGC-3'
Rev: 5'-TGCAACCCACATAAACTTCATTGC-3'

Mouse embryonal carcinoma cell line P19 were grown in MEM α (Gibco 12571-063) supplemented with 10% fetal bovine serum (FBS, Gibco 10099-141). For luciferase assay, P19 cells transfections were performed in triplicate in 24-well plates by using Fugene HD transfection reagent (Promega, E2311) according to the manufacturer's protocol. The amounts of plasmids for each transfection were: 40 ng pGL4.73 (Promega, Renilla luciferase vector), 240 ng pCS2-empty or pCS2-*Sp9*, 240 ng pGL4.23-empty (pGL4.10-empty) (Promega), or pGL4.23-Element (pGL4.10-Promoter). Dual-luciferase assay was performed with a GloMax 20/20 Luminometer (Promega). The significance was determined via t-test.

Microscopy

Bright field images (in situ hybridization results) and some fluorescent images were imaged with Olympus BX 51 microscope

using a 4 \times or 10 \times objective. Other fluorescent images were taken with the Olympus FV1000 confocal microscope system using 10 \times , 20 \times , 40 \times , or 60 \times objectives. Z-stack confocal images were reconstructed using the FV10-ASW software. All images were merged, cropped, and optimized in Photoshop CS5 without distortion of the original information.

Cell Counting

For embryonic mice, the numbers of GFP⁺ cells in E15.5 and E17.5 motor cortex were counted in 300- μ m-wide bins that spanned from the MZ to VZ. The DAPI staining was used to demarcate MZ, cortical plate (CP), intermediate zone (IZ), SVZ, and VZ. The percentage of GFP⁺ cells in each layer was calculated. We counted cells from 5 sections of each mouse and analyzed 3 mice of each genotype (*Nkx2-1-Cre*; *Sp9*^{F/+}; *Rosa-YFP* controls and *Nkx2-1-Cre*; *Sp9*^{F/LacZ}; *Rosa-YFP* conditional mutants, *Sp9*-CKOs). We also counted the numbers of Caspased-3⁺ cells in the E17.5 ventral telencephalon ($n = 3$ mice for each genotype, 3 sections per mice).

For P30 mice, the numbers of GFP⁺, GFP⁺/PV⁺, GFP⁺/SST⁺, GFP⁺/NPY⁺, and GFP⁺/CR⁺ cells in primary motor cortex were analyzed in 500- μ m-wide bins. The numbers of GFP⁺, GFP⁺/PV⁺, and GFP⁺/ChAT⁺ cells in the striatum were analyzed in a 2-mm² area ($n = 3$ mice for each genotype, 3–5 sections per mice).

Statistics

Results were calculated as mean \pm SEM (standard error of mean), and presented as fold change relative to control. Statistical significance was assessed using unpaired Student's t-test or χ^2 test. P-values less than 0.05 were considered significant.

Results

SP9 is Expressed in MGE Progenitors and Postmitotic Interneurons

We recently showed that most, if not all, cortical interneurons are derived from *Sp9-Cre* expressing cells (Zhang et al. 2016). Indeed, in the E13.5 MGE, SP9 is broadly expressed in the MGE (Fig. 1A–B''). SP9 expression begins in scattered cells in the VZ (Fig. 1B', D), and then is expressed in virtually all SVZ cells (Fig. 1A–B''). At the VZ-SVZ boundary (also known as SVZ1) (Petryniak et al. 2007), SP9 expression begins before LHX6 (Fig. 1B). Immature MGE-derived cortical interneurons migrate into the neocortex and continue to coexpress LHX6 and SP9 (Fig. 1C–C'').

To investigate *Sp9* function in the development of MGE-derived cells, we mainly used *Sp9*^{LacZ/LacZ} constitutive null mutants and *Nkx2-1-Cre*; *Sp9*^{F/LacZ} conditional (*Sp9*-CKO) mutants with or without the *Rosa-YFP* Cre reporter allele. The constitutive and conditional mutants had greatly reduced SP9 protein and *Sp9* mRNA in the MGE (Fig. 1D–G) (Zhang et al. 2016).

Sp9 is Required for the Tangential Migration of MGE-Derived Interneurons

We next examined the role of *Sp9* in the tangential migration of MGE-derived cortical inhibitory GABAergic interneurons in *Sp9*-CKOs. In E12.5 *Nkx2-1-Cre*; *Sp9*^{F/+}; *Rosa-YFP* littermate controls, many GFP⁺ cells have entered the lateral cortex (Fig. 2A, A'), whereas, in the *Sp9*-CKOs very few GFP⁺ cells were detected in this region (Fig. 2B, B'). By E13.5, a large number of GFP⁺ cells

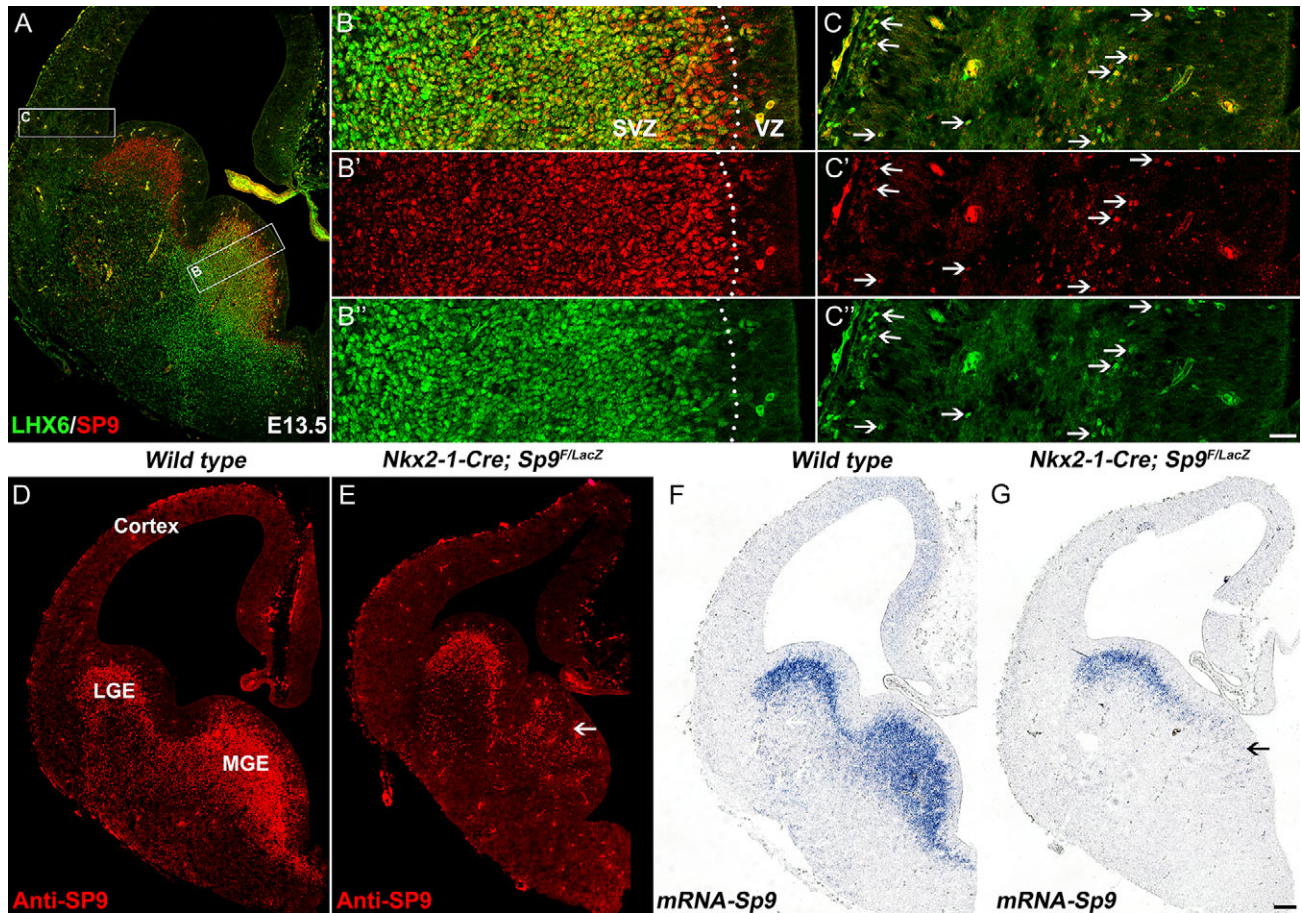


Figure 1. SP9 is expressed in LHX6⁺ MGE progenitors and derived interneurons. (A) SP9/LHX6 double-immunostained coronal hemisection at E13.5. (B, C) Higher magnification images of boxed areas in (A) showing that the vast majority of LHX6⁺ cells expressed SP9 in the MGE SVZ and cortex (arrows). Note that some SP9⁺ cells were in the MGE VZ (B). (D–F) SP9 expression was lost in most MGE cells in *Nkx2-1-Cre; Sp9^{F/LacZ}* conditional knockout mice (*Sp9*-CKOs) at E13.5 (arrows). Scale bars: 100 μm in G for A, D–G; 20 μm in C' for B–C'.

were observed in the 2 cortical migration streams in the MZ and the IZ/SVZ (Fig. 2C, C'); the *Sp9*-CKOs showed a retardation in the progression of both migration streams, and had many fewer cells in the MZ (Fig. 2D, D'). At E15.5, the *Sp9*-CKOs continued to show a retardation into the migration into the dorsomedial cortex (Fig. 3A, B). Thus, SP9 promotes the tangential migration of MGE-derived cortical interneurons.

Sp9 Mutants Have an Altered Allocation of MGE-Derived Interneurons in the Deep and Superficial Tangential Migration Pathways

We then analyzed the numbers and distribution of MGE-derived (GFP⁺) cells in the cortex of *Sp9*-CKOs at E15.5 and E17.5. The total numbers of GFP⁺ cells in E15.5 and E17.5 mutant cortex were reduced by about 30% (Fig. 3A–D, E, G), as were the percentage of GFP⁺ migrating cells in the MZ and CP (Fig. 3A1–D1, F, H). In contrast, the percentage of mutant GFP⁺ migrating cells in the cortical SVZ was increased (Fig. 3A1–D1, F, H). Notably, in control embryos, a subpopulation of GFP⁺ cells tangentially migrates through the LGE VZ/SVZ (arrows, Fig. 3A2, C2). However, very few GFP⁺ cells were detected in the LGE VZ/SVZ in *Sp9* conditional mutants at E15.5 and E17.5 (arrows, Fig. 3B2, D2, cell density was reduced roughly 2- to 3.5-fold). By contrast, within the *Sp9*-CKO LGE, there is an obvious

corridor of migrating MGE-derived cells that are probably immature interneurons (Fig. 3B, B2). Thus, overall, while the loss of *Sp9* function reduced E15.5 and E17.5 cortical interneurons in the superficial migration zone, they were increased in the deep migration zone, suggesting that *Sp9* controls the allocation of interneurons that follow these distinct pathways.

MGE-Derived Interneurons in the Cortex are Greatly Reduced in Adult *Sp9*-CKOs

At P30, we found approximately 50% reduction of GFP⁺ neocortical cells in the *Sp9*-CKO (Fig. 4E, E', F). We next quantified the numbers of GFP⁺/PV⁺, GFP⁺/SST⁺, GFP⁺/NPY⁺, and GFP⁺/CR⁺ interneurons in the primary motor cortex (Fig. 4A–D'). The *Sp9*-CKO mutants showed a > 70% reduction in GFP⁺/PV⁺ cells, and approximately 30% reduction in GFP⁺/SST⁺ cells (Fig. 4F). By contrast, GFP⁺/NPY⁺ cells were increased (Fig. 4F); GFP⁺/CR⁺ interneurons trended towards an increase (nonsignificant trend; Fig. 4F).

SP9 is mainly expressed in the MGE SVZ and migrating MGE-derived interneurons, but not in the MGE VZ, therefore we hypothesized that loss of PV⁺ and SST⁺ cortical interneurons in *Sp9*-CKOs is mainly due to migration defects, not due to reduced cell proliferation. To test this hypothesis, we bred *Sp9* floxed mice with *Lhx6*-Cre transgenic line in which Cre

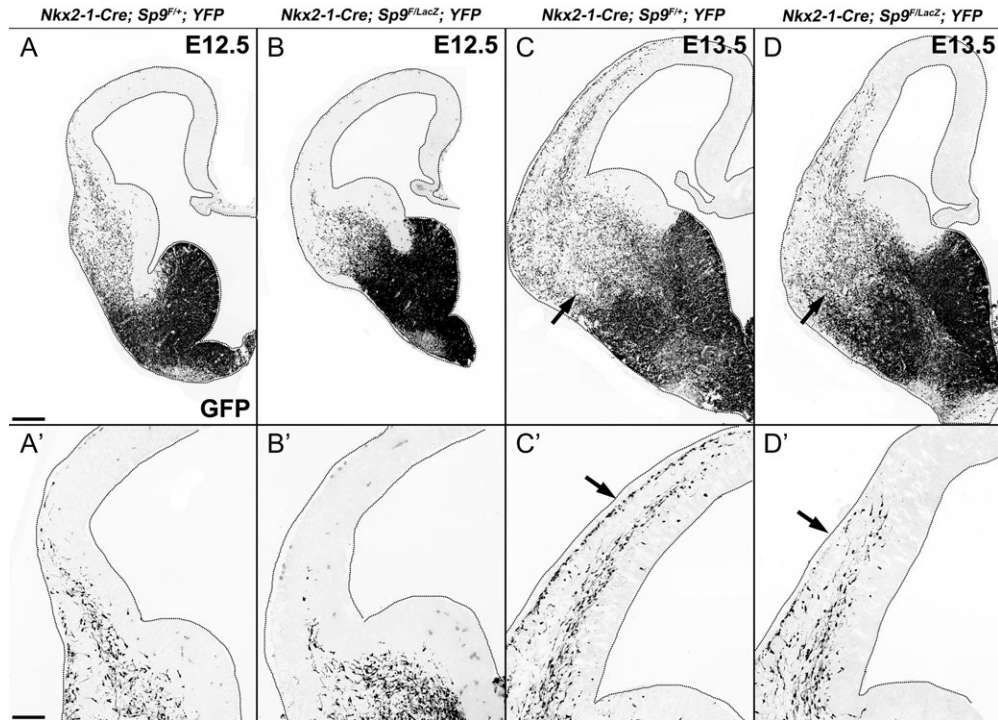


Figure 2. Tangential migration delay of MGE-derived cortical interneurons in Sp9-CKO mice. (A–D') GFP immunostaining on E12.5 and E13.5 coronal hemisections showed that MGE-derived Sp9 mutant interneurons migrate into the cortex less efficiently. Note the reduction of GFP⁺ cells in the marginal zone of Sp9-CKO mice compared with controls at E13.5 (arrows in C', D'). More GFP⁺ cells were observed in the ventral telencephalon of Sp9-CKO mice (arrows in C, D). Scale bars: 200 μm in A for A–D; 100 μm A' for A–D'.

recombination occurs only in postmitotic MGE-derived neurons (Fogarty et al. 2007; Nobrega-Pereira et al. 2008). We again quantified the numbers of GFP⁺, GFP⁺/PV⁺, GFP⁺/SST⁺, GFP⁺/NPY⁺, and GFP⁺/CR⁺ interneurons in the primary motor cortex in control (*Lhx6-Cre; Sp9^{F/+}; Rosa-YFP*) and *Lhx6-Cre; Sp9^{F/F}; Rosa-YFP* mice at P30 (Fig. 5A–E'). Consistent with results from Sp9-CKO mice (Fig. 4A–F), *Lhx6-Cre; Sp9^{F/F}; Rosa-YFP* mice showed approximately 40% reduction in GFP⁺ cells and approximately 65% reduction in GFP⁺/PV⁺ cells (Fig. 5A–F). This result suggests that SP9 only has a minor role in regulating cell proliferation in the MGE, whereas, it has a major role in promoting MGE-derived interneuron migration.

MGE-Derived Interneurons in the Striatum are Reduced in Adult Sp9-CKO Mice

MGE also generates striatal interneurons. Sp9-CKO mice had approximately 70% reduction of GFP⁺/PV⁺ and GFP⁺/SST⁺ interneurons, whereas the number of GFP⁺/ChAT⁺ cells were normal (Supplementary Fig. S1A, A', C–F'). Once again, *Lhx6-Cre; Sp9^{F/F}; Rosa-YFP* mice had a reduction of PV⁺ or SST⁺ interneurons in the striatum (Supplementary Fig. S1B, B', C, G–I'). This indicates that SP9 also promotes MGE-derived interneurons migrating into the striatum.

RNA-Seq Reveals Molecular Defects of the Sp9 Mutant MGE

Towards elucidating the mechanisms underlying the Sp9 mutant phenotypes, we used RNA-Seq to compare wild-type with Sp9 null mutant transcriptomes from the E12.5 MGE. We identified 392 dysregulated genes in the mutants; 188 with

increased RNA expression and 204 with reduced RNA expression. Some of these genes were listed in the Supplementary Table S1. We have deposited the RNA-Seq data to NCBI's GEO (GEO database GSE99049).

Differential expression was validated for several genes via in situ hybridization in E12.5–E15.5 embryos (Supplementary Figs S2, S3; Figs 6–8). For example, we observed that expression of *Zeb2*, *Maf* (*c-maf*), *Rnd2* and *St18* were greatly reduced (Supplementary Fig. S2A–L'), whereas expression of *Sp8*, *Epha3* (*Eph* receptor A3) and *Id2* were increased, and expression of *Dlx2* and *Ccnd2* (*cyclin D2*) were at the same level (Supplementary Fig. S3A–O'). Moreover, the expression of *Lhx6*, *Lhx8*, *Shh*, *Ackr3*, and *Arx* were also significantly reduced (Figs 6, 7), whereas expression of *Sst*, *Npy*, and *Sox6* were increased (Fig. 8A–O'). Overall, the altered expression patterns of these genes mainly occurred in the MGE SVZ (*Zeb2*, *Maf*, *Rnd2*, *St18*, *Sp8*, *Epha3*, *Id2*, *Lhx6*, *Lhx8*, *Ackr3*, and *Arx*) and MGE-derived migrating interneurons (*Epha3*, *Ackr3*, *Arx*, *Sst*, *Npy*, *Sox6*, and NKX2-1), consistent with the Sp9 expression pattern during embryonic development, and these genes are also known for controlling cortical interneuron development (see below).

Lhx6, *Lhx8*, *Shh*, *Ackr3*, and *Arx* expression are Reduced in the Sp9 Mutant MGE

Lhx6 and *Lhx8* have redundant functions in promoting cortical interneuron generation, in part through driving *Shh* expression and repressing *Nkx2-1* expression in MGE neurons (Flandin et al. 2011). The Sp9 mutant MGE at E12.5 showed reduced *Lhx6* expression in the SVZ (Fig. 6A–C'), reduced *Lhx8* expression in the dorsal SVZ (arrows, Fig. 6D–F') and reduced *Shh* neuronal expression in the MZ (Fig. 6G–I'). Reduced *Lhx6* and *Lhx8* SVZ expression in the

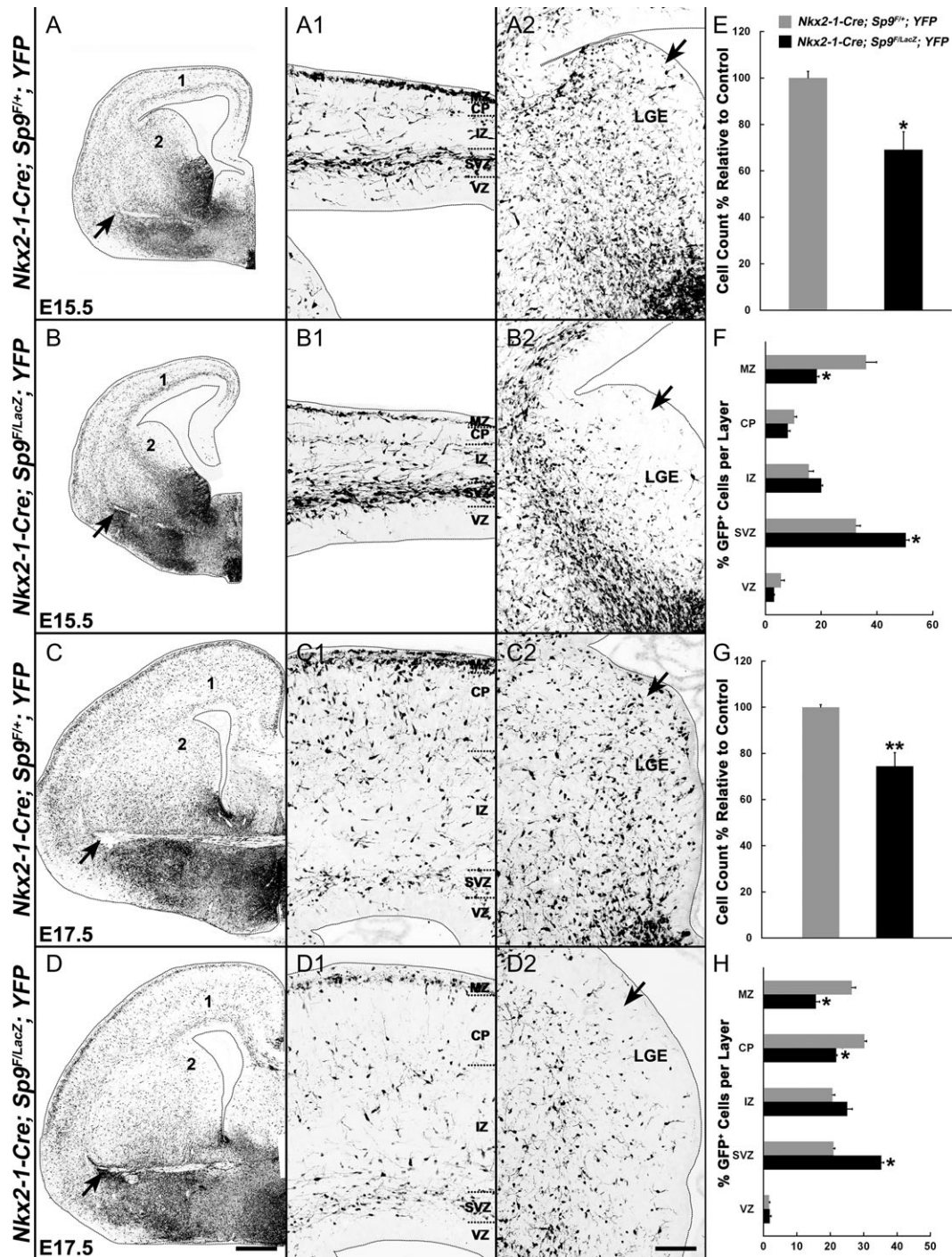


Figure 3. MGE-derived interneurons are reduced and distributed abnormally in the cortex of *Sp9*-CKOs. (A–D2) GFP immunostaining on coronal hemisections showing the distribution of MGE-derived cells (GFP⁺) in telencephalic hemispheres at E15.5 and E17.5. Note that GFP⁺ cells in the LGE VZ/SVZ of mutants were absent or greatly reduced at E15.5 and at E17.5 (arrows in A2–D2). More GFP⁺ cells were observed in the ventral telencephalon of *Sp9*-CKOs (arrows in A–D). (E–H) Quantification showing that *Sp9*-CKO mice had reduced numbers of GFP⁺ cells in the cortex at E15.5 (E) and E17.5 (G). The percentage of GFP⁺ cells was reduced in the marginal zone (MZ) and cortical plate (CP) (F, H), and increased in the SVZ (F, H). IZ, intermediate zone. Student's *t*-test (E, G) and χ^2 test (F, H), **P* < 0.05; ***P* < 0.01, *n* = 3. Scale bars: 200 μ m in D for A–D; 100 μ m D2 for A1–D2.

E13.5 and E15.5 MGE was also observed (Fig. 7A–F', M–R'). We suggest that the combined reduction of *Lhx6*, *Lhx8*, and *Shh* in the *Sp9* mutant contributes to the reduced numbers and abnormal migration of the cortical interneurons. Furthermore, we provided evidence that LHX6 directly binds to and promotes the activity of

Acr3 and *Arx* enhancers (Vogt et al. 2014). Thus, reduced *Lhx6* expression in the *Sp9* mutant MGE probably contribute to the reduced *Acr3* and *Arx* expression in the MGE SVZ (in conjunction with the reduced *Lhx8*) and in the MGE-derived migrating cortical interneurons (Fig. 7G–L' and S–U').

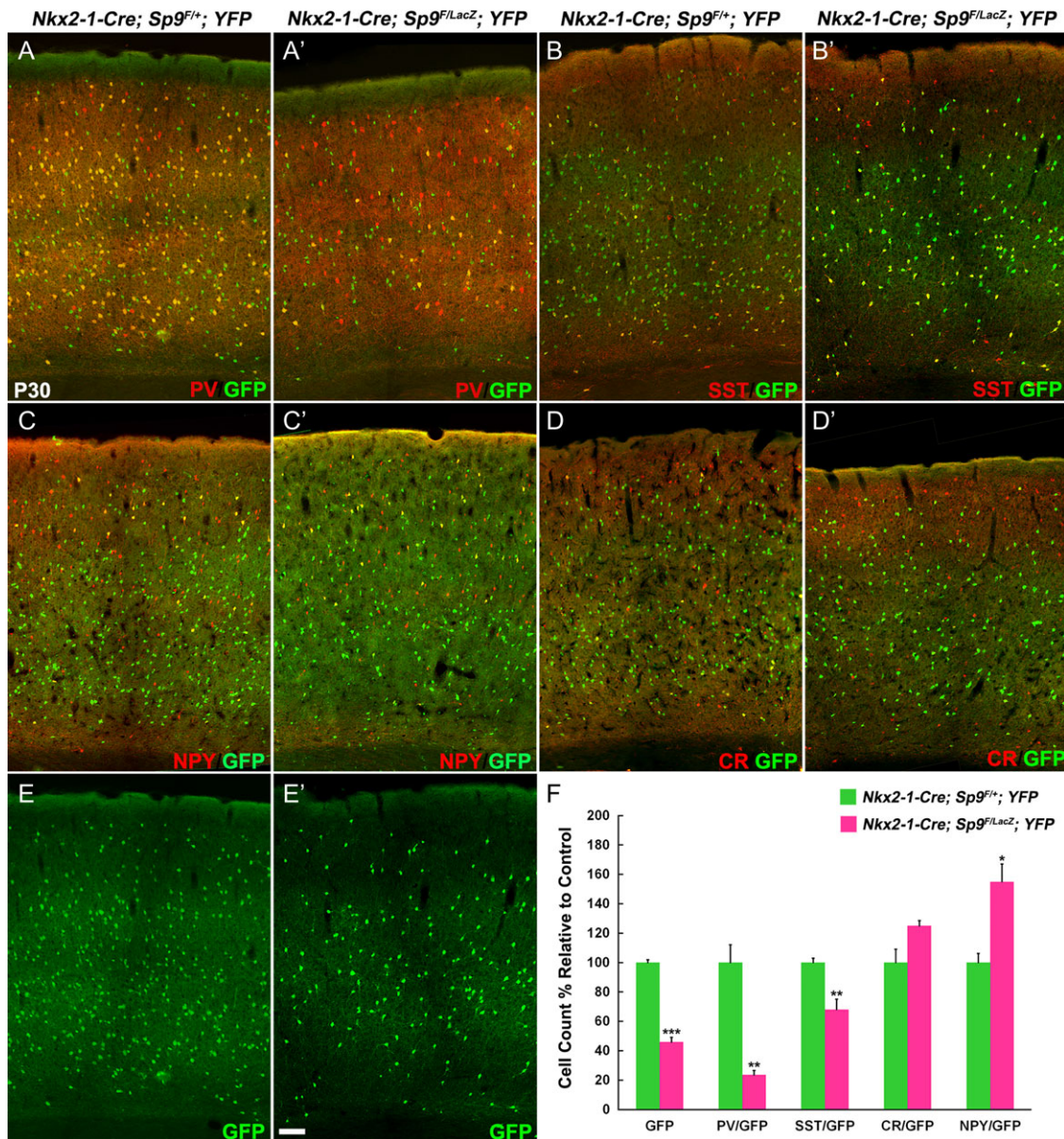


Figure 4. Cortical interneurons are reduced in *Nkx2-1-Cre; Sp9^{F/LacZ}; Rosa-YFP* conditional mutants (*Sp9*-CKOs). (A–E') GFP and interneuron markers (PV, SST, CR, and NPY) double-immunostaining on P30 cortex sections. (F) Quantification showing that *Sp9*-CKOs had reduced GFP⁺, GFP⁺/PV⁺, and GFP⁺/SST⁺ cells, and had increased GFP⁺/NPY⁺ cells in the primary motor cortex. Student's t-test, **P* < 0.05; ***P* < 0.01, ****P* < 0.001, *n* = 3. Scale bar: 50 μ m.

MGE-Derived Interneurons Ectopically Accumulate in the Ventral Telencephalon of *Sp9*-CKO Embryos

A mechanism that appears to contribute to the reduction in cortical and striatal interneurons in the *Sp9*-CKOs is the ectopic accumulation of MGE-derived cells in the ventral telencephalon appearing at E13.5, E15.5, and E17.5 (arrows, Figs 2C, D, and 3A–D). Cells in the ectopia are labeled by expression of cortical interneuron and MGE markers, including *Lhx6* (arrowheads, Fig. 7M–O'), *Npy*, *Sst*, and *Sox6* (arrows, Fig. 8A–O'). These cells also express NKX2-1 (arrows, Fig. 9D, D'), whose expression may contribute to their abnormal migration (Nobrega-Pereira et al. 2008). Upregulation of NKX2-1 expression was also observed in the LGE SVZ/MZ and cortical SVZ in *Sp9* mutants (arrows, Fig. 9D'), probably contributed by reduced *Lhx6* and *Lhx8* expression (Flandin et al. 2011). When using the *Lhx6*-Cre

line to conditionally delete *Sp9*, we also observed the ectopic accumulation of MGE-derived cells (NKX2-1⁺ and/or GFP⁺) in the ventral telencephalon (arrows, Supplementary Fig. S4A–F) and upregulation of NKX2-1 expression in the cortical SVZ (Supplementary Fig. S4C'). We found that MGE-derived interneurons expressed much higher levels of *Sst*, *Npy*, and *Sox6* in *Sp9*-CKO embryos than those in controls (arrowheads, Fig. 8A–O'). Notably, although the number of MGE-derived cortical interneurons was reduced in the cortical MZ of *Sp9* mutants (Figs 2 and 3), the remained cortical MZ interneurons also upregulated *SST* expression (arrows, Supplementary Fig. S5B').

Finally, we used *Lhx6*-GFP BAC transgenic mouse lines to examine *Lhx6*-GFP expression in the *Sp9^{LacZ/LacZ}* null mutants at E14.5. We performed GFP/LacZ double-immunostaining. In the *Lhx6*-GFP; *Sp9^{LacZ/+}* control MGE and cortex, virtually all

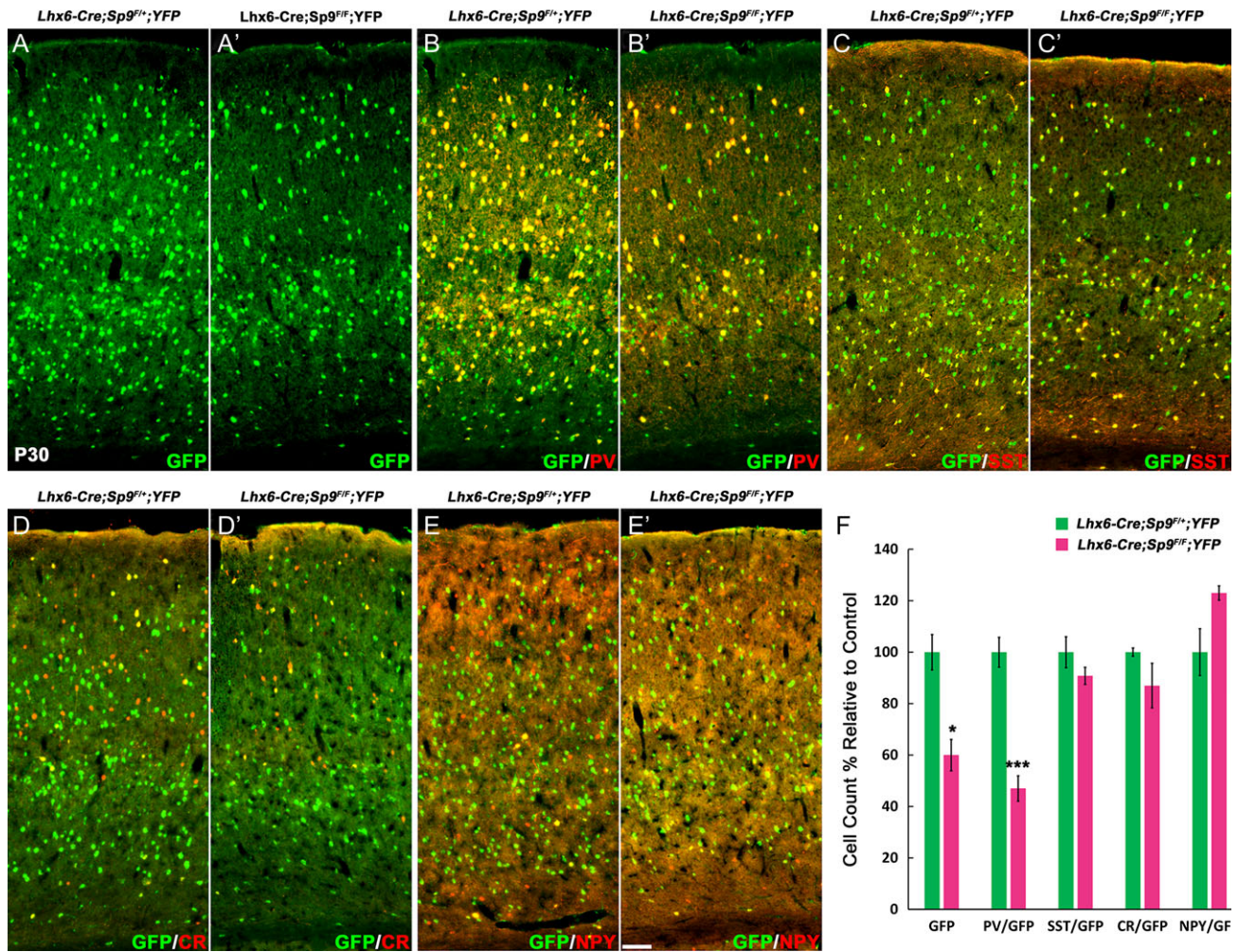


Figure 5. Cortical interneurons are reduced in *Lhx6-Cre; Sp9^{F/F}; Rosa-YFP* mice. (A–E) GFP and interneuron markers double-immunostaining on P30 cortex coronal sections. (F) Quantification of above experiments. GFP⁺ and GFP⁺/PV⁺ cells were significantly reduced. Student's t-test, **P* < 0.05; ****P* < 0.01, *n* = 3. Scale bar: 100 μ m.

Lhx6-GFP⁺ cells expressed LacZ (Supplementary Fig. S6A). *Lhx6*-GFP was strongly expressed in the globus pallidus (Supplementary Fig. S6A, C), whereas LacZ expression was downregulated in this nucleus (Supplementary Fig. S6B) (Zhang et al. 2016). In the *Lhx6-GFP; Sp9^{LacZ/LacZ}* mutant mice, LacZ expression was stronger relative to the *Lhx6-GFP; Sp9^{LacZ/+}* mice (Supplementary Fig. S6B, E), reflecting LacZ dosage. In control mice, more *Lhx6*-GFP⁺ cells were found in the MGE SVZ (Supplementary Fig. S6G), than in the mutant MGE SVZ (Supplementary Fig. S6H). *Lhx6*-GFP expression was also reduced in cells migrating through the mutant LGE VZ/SVZ (Supplementary Fig. S6G, H). Furthermore, the number of *Lhx6*-GFP⁺ interneurons in the *Sp9* mutant E14.5 cortex was reduced by 60% relative to control (Supplementary Fig. S6I).

The reduction in cortical interneurons does not appear to be caused by an increased cell death, (as marked by cleaved Caspase-3⁺ cells) as we did not observe increased cell death in the MGE, the migration streams or in the cortex of *Sp9* mutants (from E13.5 to P11). On the other hand, increased apoptosis was observed in the mutant's ventral telencephalon at E17.5 (Supplementary Fig. S7A, B, E) which may reflect the ectopic accumulation of MGE-derived interneurons. Increased apoptosis was also seen in the dorsal striatum at P3 (Supplementary Fig. S7C, D, F).

SP9 Directly Binds to a Putative Enhancer of *Lhx6*

Coexpression of SP9 and LHX6 in MGE-derived migrating interneurons from the MGE SVZ to cortex indicates that SP9 may directly regulate *Lhx6* expression. We thus performed chromatin coimmunoprecipitation followed by high-throughput DNA sequencing (ChIP-Seq) (*n* = 2 replicas) using E13.5 wild-type ganglionic eminences (LGE + MGE) (Sandberg et al. 2016; Pla et al. 2017). There was strong concordance in SP9 binding across replicates (Fig. 10A–H). We derived a set of 2962 binding regions based on the presence of significant enrichment in SP9 ChIP libraries and no enrichment in the input control datasets. Furthermore, most of those genes that were deregulated in the *Sp9* mutant MGE (Supplementary Table 1) had SP9 binding sites (Fig. 10A–H). We found one SP9 ChIP-Seq peak at the *Lhx6* promoter region and 3 peaks at *Lhx6* and *Lhx8* putative enhancers (region 1–3), as each of these loci are evolutionarily (see mammal conservation track in Fig. 10A, B).

Next, to test the ability of SP9 to regulate these candidate regulatory elements of *Lhx6* and *Lhx8*, we performed a Dual-luciferase transcription activation assay using P19 embryonal carcinoma cells. SP9 robustly activated transcription from an *Lhx6*'s putative enhancer (Region 2, Fig. 10A, I). In contrast, SP9 did not activate *Lhx6* promoter and other *Lhx6* and *Lhx8*

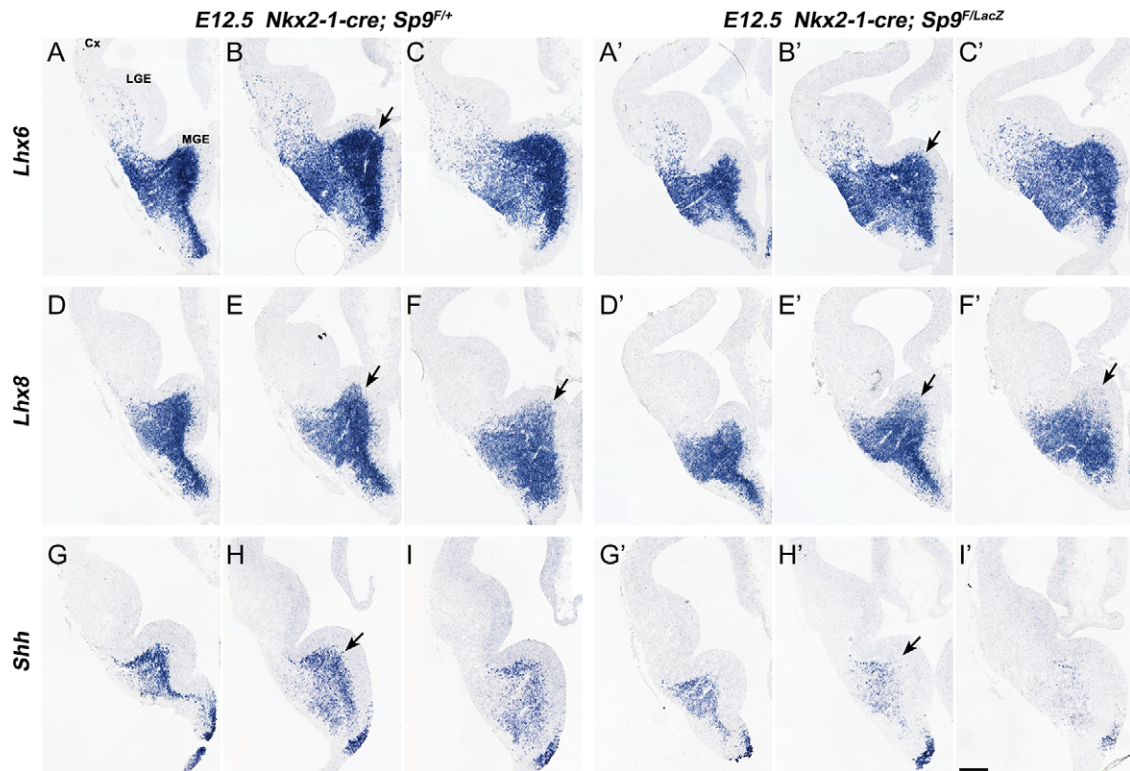


Figure 6. *Lhx6*, *Lhx8*, and *Shh* expression were downregulated in the *Sp9*-CKO MGE. (A–I) In situ RNA hybridization staining for *Lhx6*, *Lhx8*, and *Shh* on E12.5 3 serial coronal hemisections (rostral-most on the left) showed reduced *Lhx6* expression in the MGE SVZ (arrows in B, B'), reduced *Lhx8* expression in the dorsal MGE SVZ (arrows in E–F') and reduced *Shh* expression in the MGE mantle zone (MZ) of *Sp9*-CKOs (arrows in H–H'). Cx, cortex. Scale bar: 200 μ m.

enhancers in P19 embryonal carcinoma cells (Region 1 and 3) (Fig. 10I). Together, these results provide evidence that SP9 directly, at least in part, promotes *Lhx6* expression in MGE-derived migrating interneurons through its binding to an *Lhx6* enhancer.

Discussion

Here, we show that *Sp9* null and CKO mice have approximately 50% reduction in MGE-derived cortical interneurons, which we propose is mainly due to abnormal tangential migration. In the absence of *Sp9*, a subset of MGE-derived interneurons did not migrate into the cortex or striatum, resulting in their ectopic accumulation in superficial parts of the LGE and CGE and in the external capsule. In the *Sp9* mutant embryonic cortex, fewer MGE-derived interneurons migrated in the cortical MZ, whereas, more migrated in the cortical SVZ. Finally, in the *Sp9* mutant adult cortex, the SST⁺/PV⁺ ratio is increased in cortical interneurons. *Lhx6* and *Lhx8* expression are reduced in the MGE; we propose that this defect underlies, in part, the cortical interneuron defects.

Sp9 Regulates Tangential Migration of MGE-Derived Cortical Interneurons

Tangential migration to the cortex in the *Sp9* mutants appeared reduced at E13.5 and E15.5 using MGE-lineage analysis (Figs 2 and 3). The ectopic accumulation of interneuron-like cells in superficial parts of the LGE and CGE, and in the external capsule (arrows Figs 2, 3, and 7–9), appears to be a major contributor to this phenotype. The persistent expression of NKX2-1

(Fig. 9) and EphA3 (Supplementary Fig. S3D–F'), in these cells, may contribute to their abnormal migration.

Prenatally, *Sp9* mutants had a reduction of cortical interneurons in the superficial migration zone, whereas they had more cortical interneurons in the deep migration zone. Thus, *Sp9* regulates the relative allocation of interneurons that follow these distinct pathways. It is possible that interneurons migrating along these paths have different fates, in terms of their cell types and laminar positioning. This may account for why the P30 cortex had more interneurons in the superficial layers and a fewer in the deep layers (data not shown). The abnormal ratio of superficial and deep tangentially migrating interneurons may also be related to the altered ratio of PV⁺ and SST⁺ interneurons (Figs 4 and 5). Further studies are needed to establish whether *Sp9* expression in the MGE SVZ, and in the migrating interneurons, has distinct roles in regulating interneuron migration.

Normally, a subset of MGE-derived interneurons tangentially migrate into the cortex via the LGE VZ/SVZ, however, in the *Sp9*-CKOs very few GFP⁺ cells were found in this region (arrows in Fig. 3A2–D2). This could be explained by the upregulation of *Epha3* expression in the *Sp9* mutant MGE-derived migrating interneurons (Supplementary Fig. S3D–F'), as enhanced Eph/ephrin signaling in the LGE VZ/SVZ increases the repulsive effect on migrating interneurons (Zimmer et al. 2008; Rudolph et al. 2010; Villar-Cervino et al. 2015). Accordingly, in the postnatal brain, fewer GFP⁺ cells were observed in the medial part of the *Sp9* mutant striatum (Supplementary Fig. S1A, A'). Notably, Ephrin-A3 is strongly expressed in the CP (Rudolph et al. 2010). Thus, upregulation of *Epha3* expression also prevents migrating *Sp9* mutant

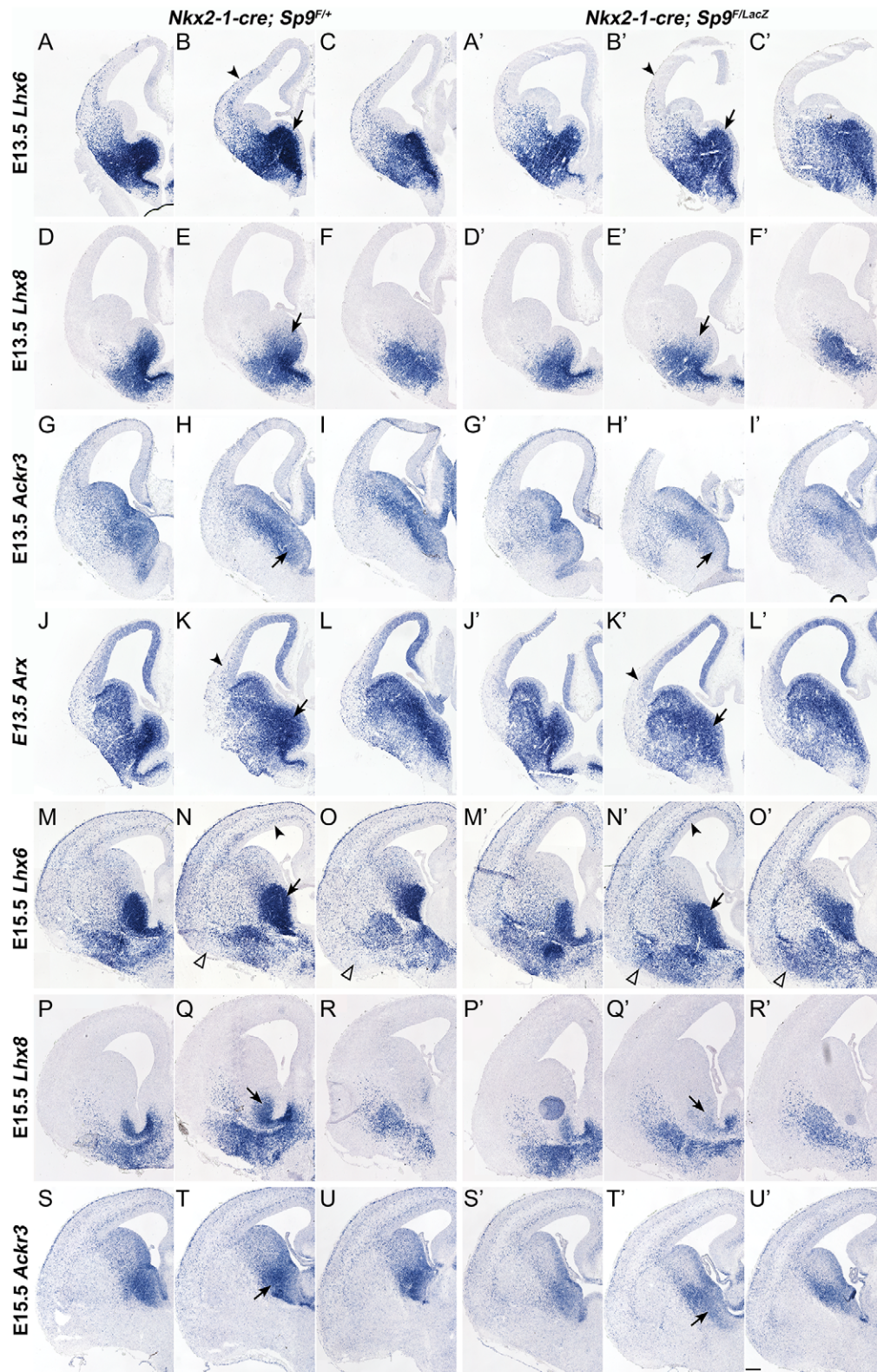


Figure 7. *Sp9*-CKOs have reduced *Lhx6*, *Lhx8*, *Akr3*, and *Arx* expression in the MGE. (A–U) In situ RNA hybridization showing that expression of *Lhx6*, *Lhx8*, and *LHX6* direct target genes, *Akr3* and *Arx*, were reduced in the mutant MGE at E13.5 and E15.5 (arrows). Arrowheads in (B, B') indicate less efficient tangential migration of *Lhx6*⁺ cortical interneurons. Arrowheads in (K, K') indicate reduced expression of *Arx* in cortical interneurons. Arrowheads in (N, N') indicate increased *Lhx6*⁺ interneurons in the *Sp9* mutant cortical SVZ. Open arrowheads in (N, N', O, O') indicate ectopic accumulation of *Lhx6*⁺ interneurons in the *Sp9* mutant ventral telencephalon. Scale bar: 200 μ m.

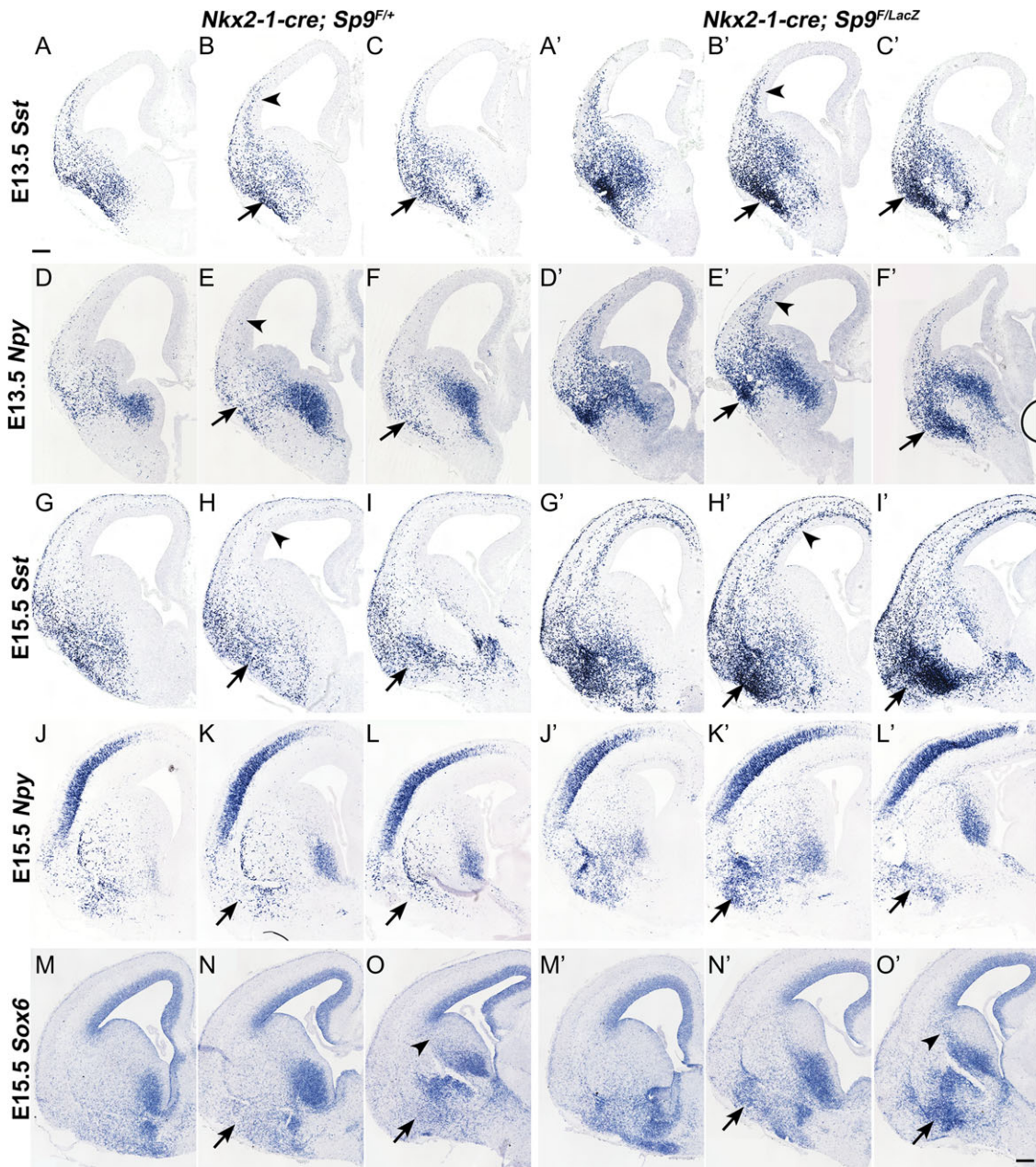


Figure 8. Ectopic accumulation of MGE-derived interneurons in the *Sp9*-CKO ventral telencephalon. (A–O') In situ RNA hybridization showing that MGE-derived *Sst*⁺, *Npy*⁺, and *Sox6*⁺ cells ectopically accumulated in the ventral telencephalon of mutants at E13.5 and E15.5 (arrows). Arrowheads in (B, B', E, E', H, H') indicate upregulation of *Sst* and *Npy* expression in *Sp9* mutant cortical interneurons. Scale bar: 200 μ m.

MGE-derived interneurons from entering the CP and pushes these interneurons into the SVZ (Fig. 3).

***Sp9* Mutants Have an Increased Ratio of SST⁺ to PV⁺ Cortical Interneurons**

Multiple transcriptional and signaling mechanisms control the specification and ratio of SST⁺ to PV⁺ cortical interneurons (Hu et al. 2017). *Sp9* mutants have an increased ratio of SST⁺ to PV⁺ cortical interneurons (Figs 4 and 5). This could be due to differential cell death, although increases in apoptosis were only observed in the area of the ectopic interneuron accumulation and in the dorsal striatum (Supplementary Fig. S7). Alternatively, *Sp9* may differentially regulate the generation of

SST⁺ and PV⁺ interneurons. This possibility seems plausible given the robust increase in SST expression in cortical immature interneurons present at E13.5–15.5 (Fig 8, Supplementary Fig. S5).

SST interneurons are generally generated before PV interneurons (Xu et al. 2004; Butt et al. 2005; Miyoshi et al. 2007), and thus, *Sp9* could alter their balance by controlling the timing of SST and PV specification. There is also evidence that SST⁺ interneurons arise via direct neurogenesis from VZ progenitors, whereas PV⁺ interneurons originate from SVZ progenitors of the MGE (Petros et al. 2015). Thus, perhaps *Sp9*, by virtue of its SVZ expression (Fig. 1), is particularly important in generating PV interneurons. Note that there is a selective deficit in cortical PV⁺ interneurons in mice lacking *Cnd2* in the SVZ of the MGE

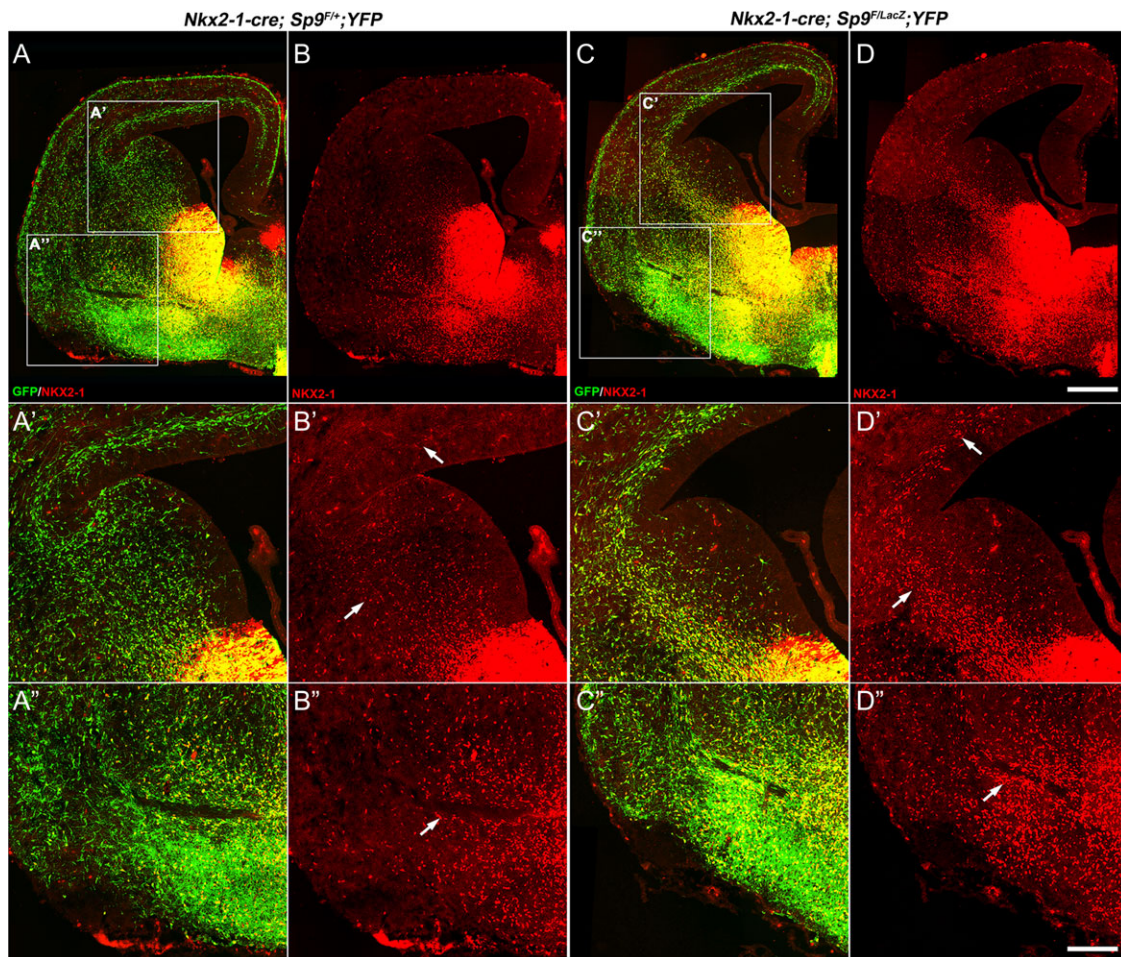


Figure 9. Upregulation of NKX2-1 in MGE-derived cells in *Sp9*-CKOs. (A–D) NKX2-1/GFP double-immunostaining on coronal hemisections at E15.5. (A–D') Higher magnification view of GFP⁺ and/or NKX2-1⁺ cells in control (*Nkx2-1-Cre; Sp9^{F/+}; Rosa-YFP*) and *Sp9*-CKOs. Note NKX2-1 upregulation in many MGE-derived migrating cortical interneurons in *Sp9*-CKOs (arrows in B', D'). (A'–D'') A large ectopic aggregation of NKX2-1⁺ cells in the ventral telencephalon of *Sp9*-CKOs (arrows in B'', D''). Scale bars: 200 μ m in (D) for (A–D); 100 μ m in (D'') for (A'–D'').

(Glickstein et al. 2007); however, *Cnd2* expression was not affected in the *Sp9* mutant MGE, according to our RNA-Seq and in situ hybridization analysis (Supplementary Fig. S3M–O).

Sp9 Regulation of Multiple Transcription Factors Controls Cortical Interneuron Development

There is evidence dorsal MGE has a bias for generating SST cortical interneurons whereas the ventral MGE has a bias for generating PV interneurons and the globus pallidus (Flandin et al. 2010; Nobrega-Pereira et al. 2010; Inan et al. 2012). Although *Sp9* expression appears uniform across the MGE, development of pallidal projection neurons (e.g., globus pallidus) appears grossly normal, perhaps because *Sp9* is not expressed in these neurons (Zhang et al. 2016). On the other hand, the *Sp9* mutants have reduced numbers of both striatal and cortical interneurons (Figs 4 and 5; Supplementary Fig. S1). The specificity for MGE-derived interneurons, and the increase in the cortical interneuron SST/PV ratio, may reflect the combination of transcription factors that are altered in the *Sp9* mutants.

Sp9 mutants have reduced expression of the *Lhx6*, *Lhx8*, *Zeb2*, and *Maf* transcription factors. Reductions in both *Lhx6* and *Lhx8* could explain why both cortical and striatal interneurons are affected (Flandin et al. 2011). The lack of a defect in striatal

cholinergic neurons (Supplementary Fig. S1), which require *Lhx8* function LGE (Zhao et al. 2003), implies further specificity of *Sp9*'s function. *Dlx1&2* and *Zeb2* mutants fail to express the *Maf* and *Mafb* transcription factors, whose expression is highly enriched in developing cortical interneurons (McKinsey et al. 2013). Downregulation of *Zeb2* expression could explain why NKX2-1 expression was upregulated in several MGE derivatives: the ectopic interneurons in the superficial LGE, and interneurons migrating through the LGE SVZ and cortical SVZ (Fig. 9). *Dlx1&2* control the generation of cortical interneurons through increasing expression of the *Zeb2* transcription factor in the SVZ of the MGE, which in turn represses *Nkx2-1* expression (McKinsey et al. 2013; van den Berghe et al. 2013). Thus, we propose that reduced expression of *Lhx6*, *Lhx8*, *Zeb2*, and *Maf* in the *Sp9* mutant together contribute to the defects in cortical interneuron development.

To investigate whether these genes are directly regulated by SP9, we performed SP9 ChIP-seq using E13.5 ganglionic eminences. We found that SP9 binds to loci in the region of genes dysregulated in the *Sp9* mutant: *AckR3*, *Arx*, *EphA3*, *Lhx6*, *Lhx8*, *Nkx2-1*, *St18*, and *Zeb2* (Fig. 10A–H). Thus, *Sp9*, through direct activation (*AckR3*, *Arx*, *Lhx6*, *Lhx8*, *St18*, and *Zeb2*) and repression (*Nkx2-1* and *EphA3*), has multiple molecular targets, and modes of function, in regulating development of MGE-derived cortical

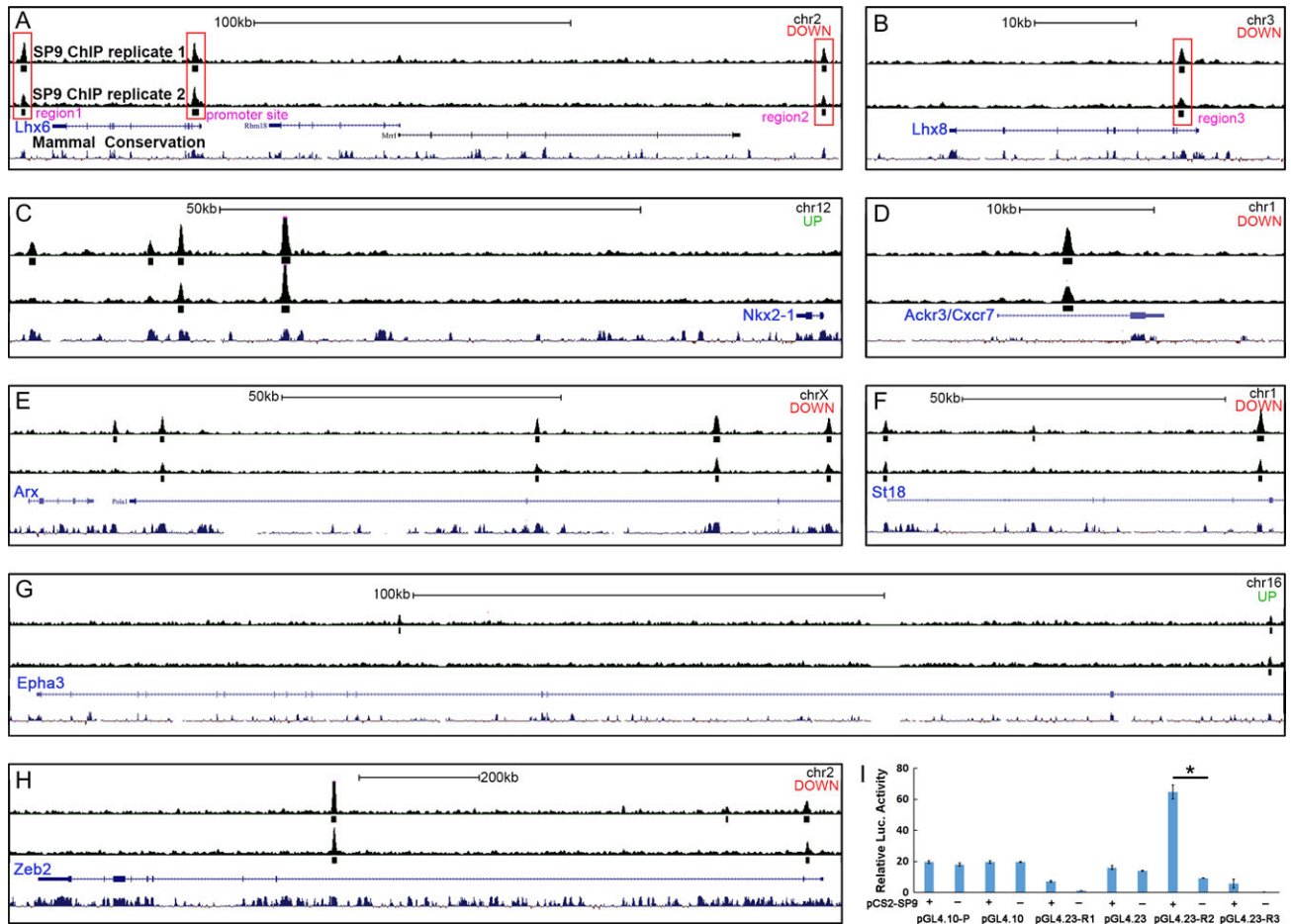


Figure 10. Anti-SP9 ChIP-Seq Results. (A–H) “Called” peak (small rectangles) locations relative to genomic loci are shown for genes that are deregulated in Sp9-CKOs and for which ChIP-seq peaks were identified within 1 Mb of the gene body. Note the different scale bars for individual panels. For each panel, “up” or “down” indicates whether the gene was upregulated or downregulated in the Sp9 mutant MGE. chr, chromosome; kb, kilobase. Large red rectangles highlight where SP9 binds to the promoter and several downstream or upstream regions (regions 1–3) of *Lhx6* and *Lhx8* genes (A, B). (I) SP9 activated transcription from a putative *Lhx6* enhancer (R2, region 2) in a dual-luciferase assay within P19 cells. (Student’s t-test, * $P < 0.05$, $n = 3$ individuals, mean \pm SEM).

interneurons. As discussed above, this function appears to be particularly important of interneuron tangential migration. In this regard we recently demonstrated that *Sp9* and *Sp8* in the dLGE and postnatal SVZ also have critical roles in promoting migration of olfactory bulb interneurons (Li et al. 2017).

Most *Lhx6* mutant MGE-derived cortical interneurons fail to differentiate to mature PV⁺ and SST⁺ interneurons, while this defect was not observed in *Sp9* mutants. However, *Sp9* mutants partially phenocopy the migration defects of MGE-derived interneurons in *Lhx6* and *Lhx6/Lhx8* mutants (Liodis et al. 2007; Zhao et al. 2008; Flandin et al. 2011; Vogt et al. 2014). A putative *Lhx6* enhancer (Region 2 in Fig. 10A) was strongly activated by SP9 in luciferase reporter assays. Given that enhancers are required for normal development (Dickel et al. 2018), our results suggest that the *Lhx6* enhancer may have a crucial role in promoting the tangential migration of MGE-derived interneurons.

Authors’ Contributions

Z.L. and Z.Z. performed experiments and analysis. S.L. performed SP9 ChIP-Seq. Z.L., Z.X., S.W., Q.L., Y.W., G.T., and Y.Y. helped conduct experiments and analyze the data. B.C., Y.W., and J.L.R. helped guide the project and discussed some of the

results. Z.Y. designed the experiments and analyzed the results. Z.Y. and J.L.R. wrote the article.

Supplementary Material

Supplementary material are available at *Cerebral Cortex* online.

Funding

Research grants to Z.Y. from the National Natural Science Foundation of China (NSFC 31630032, 31425011, and 31429002), research grant to Y.Y. (NSFC 31700889), research grants to B.C. from NIH (MH094589 and NS089777), and J.L. Rubenstein from NIH (MH049428).

Notes

The GEO accession number for the RNA-Seq data reported in this article is GSE 99 049. Conflict of Interest: J.L.R. is cofounder, stockholder, and currently serve on the scientific board of Neurona, a company studying the potential therapeutic use of interneuron transplantation. *Conflict of interest:* none declared.

References

- Alifragis P, Liapi A, Parnavelas JG. 2004. Lhx6 regulates the migration of cortical interneurons from the ventral telencephalon but does not specify their GABA phenotype. *J Neurosci.* 24:5643–5648.
- Anderson SA, Eisenstat DD, Shi L, Rubenstein JL. 1997. Interneuron migration from basal forebrain to neocortex: dependence on Dlx genes. *Science.* 278:474–476.
- Brown KN, Chen S, Han Z, Lu CH, Tan X, Zhang XJ, Ding L, Lopez-Cruz A, Saur D, Anderson SA, et al. 2011. Clonal production and organization of inhibitory interneurons in the neocortex. *Science.* 334:480–486.
- Butt SJ, Fuccillo M, Nery S, Noctor S, Kriegstein A, Corbin JG, Fishell G. 2005. The temporal and spatial origins of cortical interneurons predict their physiological subtype. *Neuron.* 48:591–604.
- Dickel DE, Ypsilanti AR, Pla R, Zhu Y, Barozzi I, Mannion BJ, Khin YS, Fukuda-Yuzawa Y, Plajzer-Frick I, Pickle CS, et al. 2018. Ultraconserved enhancers are required for normal development. *Cell.* 172:491–499 e415.
- Du T, Xu Q, Ocbina PJ, Anderson SA. 2008. NKX2.1 specifies cortical interneuron fate by activating Lhx6. *Development.* 135:1559–1567.
- Flandin P, Kimura S, Rubenstein JL. 2010. The progenitor zone of the ventral medial ganglionic eminence requires Nkx2-1 to generate most of the globus pallidus but few neocortical interneurons. *J Neurosci.* 30:2812–2823.
- Flandin P, Zhao Y, Vogt D, Jeong J, Long J, Potter G, Westphal H, Rubenstein JL. 2011. Lhx6 and Lhx8 coordinately induce neuronal expression of Shh that controls the generation of interneuron progenitors. *Neuron.* 70:939–950.
- Fogarty M, Grist M, Gelman D, Marin O, Pachnis V, Kessaris N. 2007. Spatial genetic patterning of the embryonic neuroepithelium generates GABAergic interneuron diversity in the adult cortex. *J Neurosci.* 27:10935–10946.
- Fragkouli A, Hearn C, Errington M, Cooke S, Grigoriou M, Bliss T, Stylianopoulou F, Pachnis V. 2005. Loss of forebrain cholinergic neurons and impairment in spatial learning and memory in LHX7-deficient mice. *Eur J Neurosci.* 21:2923–2938.
- Fragkouli A, van Wijk NV, Lopes R, Kessaris N, Pachnis V. 2009. LIM homeodomain transcription factor-dependent specification of bipotential MGE progenitors into cholinergic and GABAergic striatal interneurons. *Development.* 136:3841–3851.
- Gelman DM, Marin O. 2010. Generation of interneuron diversity in the mouse cerebral cortex. *Eur J Neurosci.* 31:2136–2141.
- Glickstein SB, Moore H, Slowinska B, Racchumi J, Suh M, Chuhma N, Ross ME. 2007. Selective cortical interneuron and GABA deficits in cyclin D2-null mice. *Development.* 134:4083–4093.
- Hoch RV, Lindtner S, Price JD, Rubenstein JL. 2015. OTX2 transcription factor controls regional patterning within the medial ganglionic eminence and regional identity of the septum. *Cell Rep.* 12:482–494.
- Hu JS, Vogt D, Sandberg M, Rubenstein JL. 2017. Cortical interneuron development: a tale of time and space. *Development.* 144:3867–3878.
- Inan M, Welagen J, Anderson SA. 2012. Spatial and temporal bias in the mitotic origins of somatostatin- and parvalbumin-expressing interneuron subgroups and the chandelier subtype in the medial ganglionic eminence. *Cereb Cortex.* 22:820–827.
- Li J, Wang C, Zhang Z, Wen Y, An L, Liang Q, Xu Z, Wei S, Li W, Guo T, et al. 2017. Transcription factors Sp8 and Sp9 coordinately regulate olfactory bulb interneuron development. *Cereb Cortex.* 1–17.
- Liodis P, Denaxa M, Grigoriou M, Akufo-Addo C, Yanagawa Y, Pachnis V. 2007. Lhx6 activity is required for the normal migration and specification of cortical interneuron subtypes. *J Neurosci.* 27:3078–3089.
- Long JE, Cobos I, Potter GB, Rubenstein JL. 2009. Dlx1&2 and Mash1 transcription factors control MGE and CGE patterning and differentiation through parallel and overlapping pathways. *Cereb Cortex.* 19(Suppl 1):i96–i106.
- Long JE, Swan C, Liang WS, Cobos I, Potter GB, Rubenstein JL. 2009. Dlx1&2 and Mash1 transcription factors control striatal patterning and differentiation through parallel and overlapping pathways. *J Comp Neurol.* 512:556–572.
- Marin O, Anderson SA, Rubenstein JL. 2000. Origin and molecular specification of striatal interneurons. *J Neurosci.* 20:6063–6076.
- McKinsey GL, Lindtner S, Trzcinski B, Visel A, Pennacchio LA, Huylebroeck D, Higashi Y, Rubenstein JL. 2013. Dlx1&2-dependent expression of Zfhx1b (Sip1, Zeb2) regulates the fate switch between cortical and striatal interneurons. *Neuron.* 77:83–98.
- Miyoshi G, Butt SJ, Takebayashi H, Fishell G. 2007. Physiologically distinct temporal cohorts of cortical interneurons arise from telencephalic Olig2-expressing precursors. *J Neurosci.* 27:7786–7798.
- Neves G, Shah MM, Liodis P, Achimastou A, Denaxa M, Roalfe G, Sesay A, Walker MC, Pachnis V. 2013. The LIM homeodomain protein Lhx6 regulates maturation of interneurons and network excitability in the mammalian cortex. *Cereb Cortex.* 23:1811–1823.
- Nobrega-Pereira S, Gelman D, Bartolini G, Pla R, Pierani A, Marin O. 2010. Origin and molecular specification of globus pallidus neurons. *J Neurosci.* 30:2824–2834.
- Nobrega-Pereira S, Kessaris N, Du T, Kimura S, Anderson SA, Marin O. 2008. Postmitotic Nkx2-1 controls the migration of telencephalic interneurons by direct repression of guidance receptors. *Neuron.* 59:733–745.
- Nord AS, Pattabiraman K, Visel A, Rubenstein JL. 2015. Genomic perspectives of transcriptional regulation in forebrain development. *Neuron.* 85:27–47.
- Petros TJ, Bultje RS, Ross ME, Fishell G, Anderson SA. 2015. Apical versus basal neurogenesis directs cortical interneuron subclass fate. *Cell Rep.* 13:1090–1095.
- Petryniak MA, Potter GB, Rowitch DH, Rubenstein JL. 2007. Dlx1 and Dlx2 control neuronal versus oligodendroglial cell fate acquisition in the developing forebrain. *Neuron.* 55:417–433.
- Pla R, Stanco A, Howard MA, Rubin AN, Vogt D, Mortimer N, Cobos I, Potter GB, Lindtner S, Price JD, et al. 2017. Dlx1 and Dlx2 promote interneuron GABA synthesis, synaptogenesis, and dendritogenesis. *Cereb Cortex.* doi: 10.1093/cercor/bhx241. [Epub ahead of print]
- Rubin AN, Alfonsi F, Humphreys MP, Choi CK, Rocha SF, Kessaris N. 2010. The germinal zones of the basal ganglia but not the septum generate GABAergic interneurons for the cortex. *J Neurosci.* 30:12050–12062.
- Rudolph J, Zimmer G, Steinecke A, Barchmann S, Bolz J. 2010. Ephrins guide migrating cortical interneurons in the basal telencephalon. *Cell Adh Migr.* 4:400–408.
- Rudy B, Fishell G, Lee S, Hjerling-Leffler J. 2011. Three groups of interneurons account for nearly 100% of neocortical GABAergic neurons. *Dev Neurobiol.* 71:45–61.

- Sandberg M, Flandin P, Silberberg S, Su-Feher L, Price JD, Hu JS, Kim C, Visel A, Nord AS, Rubenstein JL. 2016. Transcriptional networks controlled by NKX2-1 in the development of forebrain GABAergic neurons. *Neuron*. 91:1260–1275.
- Silberberg SN, Taher L, Lindtner S, Sandberg M, Nord AS, Vogt D, McKinsey GL, Hoch R, Pattabiraman K, Zhang D, et al. 2016. Subpallial enhancer transgenic lines: a data and tool resource to study transcriptional regulation of GABAergic cell fate. *Neuron*. 92:59–74.
- Srinivas S, Watanabe T, Lin CS, Williams CM, Tanabe Y, Jessell TM, Costantini F. 2001. Cre reporter strains produced by targeted insertion of EYFP and ECFP into the ROSA26 locus. *BMC Dev Biol*. 1:4.
- Sussel L, Marin O, Kimura S, Rubenstein JL. 1999. Loss of Nkx2.1 homeobox gene function results in a ventral to dorsal molecular respecification within the basal telencephalon: evidence for a transformation of the pallidum into the striatum. *Development*. 126:3359–3370.
- Taniguchi H, Lu J, Huang ZJ. 2013. The spatial and temporal origin of chandelier cells in mouse neocortex. *Science*. 339:70–74.
- Trapnell C, Roberts A, Goff L, Pertea G, Kim D, Kelley DR, Pimentel H, Salzberg SL, Rinn JL, Pachter L. 2012. Differential gene and transcript expression analysis of RNA-seq experiments with TopHat and Cufflinks. *Nat Protoc*. 7:562–578.
- van den Berghe V, Stappers E, Vandesande B, Dimidschstein J, Kroes R, Francis A, Conidi A, Lesage F, Dries R, Cazzola S, et al. 2013. Directed migration of cortical interneurons depends on the cell-autonomous action of Sip1. *Neuron*. 77:70–82.
- Villar-Cervino V, Kappeler C, Nobrega-Pereira S, Henkemeyer M, Rago L, Nieto MA, Marin O. 2015. Molecular mechanisms controlling the migration of striatal interneurons. *J Neurosci*. 35:8718–8729.
- Vogt D, Hunt RF, Mandal S, Sandberg M, Silberberg SN, Nagasawa T, Yang Z, Baraban SC, Rubenstein JL. 2014. Lhx6 directly regulates Arx and CXCR7 to determine cortical interneuron fate and laminar position. *Neuron*. 82:350–364.
- Wang C, You Y, Qi D, Zhou X, Wang L, Wei S, Zhang Z, Huang W, Liu Z, Liu F, et al. 2014. Human and monkey striatal interneurons are derived from the medial ganglionic eminence but not from the adult subventricular zone. *J Neurosci*. 34:10906–10923.
- Wonders CP, Anderson SA. 2006. The origin and specification of cortical interneurons. *Nat Rev Neurosci*. 7:687–696.
- Xu Q, Cobos I, De La Cruz E, Rubenstein JL, Anderson SA. 2004. Origins of cortical interneuron subtypes. *J Neurosci*. 24:2612–2622.
- Xu Q, Tam M, Anderson SA. 2008. Fate mapping Nkx2.1-lineage cells in the mouse telencephalon. *J Comp Neurol*. 506:16–29.
- Zhang Q, Zhang Y, Wang C, Xu Z, Liang Q, An L, Li J, Liu Z, You Y, He M, et al. 2016. The zinc finger transcription factor Sp9 is required for the development of striatopallidal projection neurons. *Cell Rep*. 16:1431–1444.
- Zhao Y, Flandin P, Long JE, Cuesta MD, Westphal H, Rubenstein JL. 2008. Distinct molecular pathways for development of telencephalic interneuron subtypes revealed through analysis of Lhx6 mutants. *J Comp Neurol*. 510:79–99.
- Zhao Y, Marin O, Hermes E, Powell A, Flames N, Palkovits M, Rubenstein JL, Westphal H. 2003. The LIM-homeobox gene Lhx8 is required for the development of many cholinergic neurons in the mouse forebrain. *Proc Natl Acad Sci USA*. 100:9005–9010.
- Zimmer G, Garcez P, Rudolph J, Niehage R, Weth F, Lent R, Bolz J. 2008. Ephrin-A5 acts as a repulsive cue for migrating cortical interneurons. *Eur J Neurosci*. 28:62–73.